A Solution-Phase Bifunctional Catalyst for Lithium-Oxygen Batteries

ARTICLE *in* JOURNAL OF THE AMERICAN CHEMICAL SOCIETY · MAY 2014

Impact Factor: 12.11 · DOI: 10.1021/ja501877e · Source: PubMed

11 AUTHORS, INCLUDING:

Dan Sun
Huazhong University of Science and Techn…
4 PUBLICATIONS **97** CITATIONS
SEE PROFILE

Wang Zhang
Huazhong University of Science and Techn…
3 PUBLICATIONS **167** CITATIONS
SEE PROFILE

Yunhui Huang
Huazhong University of Science and Techn…
237 PUBLICATIONS **6,388** CITATIONS
SEE PROFILE

Deli Wang
Huazhong University of Science and Techn…
43 PUBLICATIONS **1,331** CITATIONS
SEE PROFILE

JACS
JOURNAL OF THE AMERICAN CHEMICAL SOCIETY

Article

A Solution-Phase Bifunctional Catalyst for Lithium-oxygen Batteries

Dan Sun, Yue Shen, Wang Zhang, Ling Yu, Ziqi Yi, Wei Yin, Duo Wang, Yunhui Huang, Jie Wang, Deli Wang, and John B. Goodenough

J. Am. Chem. Soc., **Just Accepted Manuscript** • Publication Date (Web): 14 May 2014

Just Accepted

Journal of the American Chemical Society is published by the American Chemical Society. 1155 Sixteenth Street N.W., Washington, DC 20036

A Solution-Phase Bifunctional Catalyst for Lithium-oxygen Batteries

Dan Sun†, Yue Shen†,*, Wang Zhang†, Ling Yu†, Ziqi Yi†, Wei Yin†, Duo Wang†, Yunhui Huang†,*, Jie Wang§, Deli Wang§ and John B. Goodenough‡

† State Key Laboratory of Material Processing and Die & Mould Technology, School of Materials Science and Engineering, Huazhong University of Science and Technology, Wuhan, Hubei 430074, China

§ School of Chemistry and Chemical Engineering, Key Laboratory of Large-Format Battery Materials and System, Ministry of Education, Huazhong University of Science and Technology, Wuhan, Hubei 430074, China

‡ Texas Materials Institute, ETC 9.102, 1 University Station, C2200, The University of Texas at Austin, Austin, TX 78712, USA

Lithium-air battery , Iron phthalocyanine , Redox shuttle , Oxygen reduction reaction , Organic electrolyte

ABSTRACT: A lithium-oxygen battery would deliver the highest energy density of a rechargeable battery, but the multiphase electrochemical reaction on the air cathode is difficult to proceed when operated with only solid catalysts. We report here organic-electrolyte-dissolved iron phthalocyanine (FePc) as a shuttle of $(O_2)^-$ species and electrons between the surface of the electronic conductor and the insulator Li_2O_2 product of discharge. The Li_2O_2 is observed to grow and decompose without direct contact with carbon, which greatly enhances the electrochemical performance. Our results signal that the use of molecular shuttles which are catalytically active may prove an enabler of a practical lithium-air rechargeable battery.

INTRODUCTION

The lithium-oxygen battery has received world-wide attention because it promises the theoretical reversible high-capacity limit for a rechargeable battery[1-4]. The cathode of a lithium-oxygen cell requires a catalyst that is active for both the oxygen-reduction and oxygen-evolution reactions (ORR and OER). Many solid cathode catalysts have been developed in lithium-oxygen batteries[5,6], such as noble metals[7,8], metal oxides[7,9-14], Fe-N/C complexes[1,15-17], carbon nanotubes/nanofibers[18-21], graphene nanosheets[22-25], perovskites[26,27], pyrochlore[28], et al. However, there are still some fundamental problems remaining for solid catalysts[29]. For example, since the discharge product Li_2O_2 is also in solid state, it will accumulate at the catalyst surface and hence block the electrode reactions during the discharge process. Meanwhile, during the charging process, it is also difficult to make good contact between the solid catalyst and Li_2O_2[30,31]. Theoretically, the above problems will be alleviated if a solution-phase catalyst is used to catalyze the formation and decomposition of the solid Li_2O_2. A very recent work showed that incorporation of a redox mediator greatly improved the charging performance of the Li-O_2 battery[32,33]. But so far, the solution-phase catalysis is still an unexplored field.

In this work, we report organic-electrolyte-dissolved iron phthalocyanine (FePc) as the catalyst for both discharge and charge processes in lithium-oxygen batteries. It acts not only as a redox mediator, but also as a molecular shuttle of $(O_2)^-$ species between the surface of the electronic conductor and the insulator Li_2O_2 product of discharge.

RESULTS

Electrochemical Properties of FePc

Although it is well-known that molecular FePc is active for the ORR[34-37], FePc is not soluble in aqueous electrolytes and has a poor electronic conductivity; therefore, it is not applicable in conventional proton-exchange membrane (PEM) fuel cells. However, FePc can be dissolved in some organic electrolytes such as dimethyl sulphoxide (DMSO)[30,38] and tetraethylene glycol dimethyl ether (TEGDME)[39,40], as seen in Fig. 1a; it can be used in a lithium-air cell. If we induce some O_2 or LiOOLi powder to the diluted FePc solution, we will observe a red shift of the UV-vis absorption peak, indicating that dissolved FePc is easy to coordinate with O_2 and LiOOLi (Fig. 1b)[41].

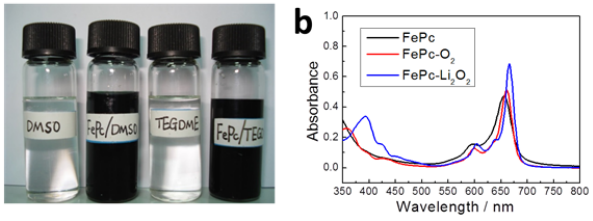

Figure 1. The electrochemical properties of FePc. (**a**) Photo of the DMSO and TEGDME electrolytes with or without 0.002 mol L^{-1} FePc. (**b**) UV-Vis absorption spectra of the FePc, FePc-O_2 and FePc-LiOOLi (1.5 x 10^{-5} mol L^{-1}).

In the absence of oxygen, the cyclic voltammetry of FePc (Fig. 2a & e) reveals two redox reactions, a complex Fe^{III}/Fe^{II} reaction near 3.65 V versus Li^+/Li^o and an Fe^{II}/Fe^{I} near 2.5 V[36,42]. In the presence of oxygen, the FePc coordinates with oxygen, and the Fe^{II}/Fe^{I} reaction shifts to 2.86 V (Fig. 2a). The $(FePc\text{-}O_2)^o/(FePc\text{-}O_2)^-$ transition can be regarded as the result of both Fe^{II}/Fe^{I} reaction and oxygen-reduction reaction. $(FePc\text{-}O_2)^-$ has several resonance structures because of the delocalization of the negative charge. If the negative charge is on the Fe atom, it can be viewed as Fe(I); if the negative charge is on the O_2 ligand, it can be viewed as a reduced oxygen. Similar to some natural enzymes with transition metal and macrocyclic ligand[43], the $(FePc\text{-}O_2)^-$ can be further reduced into $(FePc\text{-}O_2)^{2-}$ and combine with two lithium ions to form FePc-LiOOLi. The LiOOLi may dissociate from the FePc, nucleate in the electrolyte and then the FePc can catalyze the reduction of another oxygen molecule.

The ORR activity testing was performed on the rotating disk electrode (RDE). As shown in Fig. 2b, the onset potential positive shifts significantly with the existence of FePc in the solution, indicative of excellent electrocatalytic activity of FePc for ORR. With FePc, the ORR polarization curve shows two stages (Fig. 2c), agreeing with the "$(FePc\text{-}O_2) \rightarrow (FePc\text{-}O_2)^- \rightarrow$ (FePc-LiOOLi)" two-step mechanism. By using the Levich equation, the number of electrons transferred in the first step reaction is estimated to $1.14 \approx 1$ if we assume that the diffusion coefficient of FePc and $FePc\text{-}O_2$ in DMSO are same (the calculation is described in detail in the supporting information). Another interesting phenomenon is the "LiOOLi blocking effect" in the low potential region. In the system without FePc, at a rotation rate of 1600 rpm, the current density decreased when the potential was scanned below 2.33 V. This unusual phenomenon is because the reaction product, solid LiOOLi, accumulated on the electrode surface and deactivated the electrode. To confirm this point, the current was measured at fixed potential 2.40 V (Fig. 2d). Without FePc, the current decreased to close zero because of LiOOLi blocking. On the contrary, with FePc, the current was much larger because the FePc-LiOOLi compound is soluble; the LiOOLi may nucleate away from the carbon surface. The LiOOLi blocking effect is also confirmed in Fig. S1 and S2.

The FePc coordination complex can be oxidized and reduced around 3.65 V (Fig. 2e). It may serve as a shuttle to transfer the charge from the electrode surface to the lithium peroxide in the OER process. A RDE experiment with additional lithium peroxide powder demonstrates the contribution of FePc to the oxidation current (Fig. 2f). Without FePc, although Li_2O_2 particles were suspended in the electrolyte, there was no current because of the poor contact between the electrode and Li_2O_2. This is a common problem for OER in lithium-oxygen batteries. With FePc, the oxidation current increased significantly. The oxidation current in the OER potential range is not sensitive to the oxygen. The detailed catalytic mechanism of FePc for OER will be discussed in the later section.

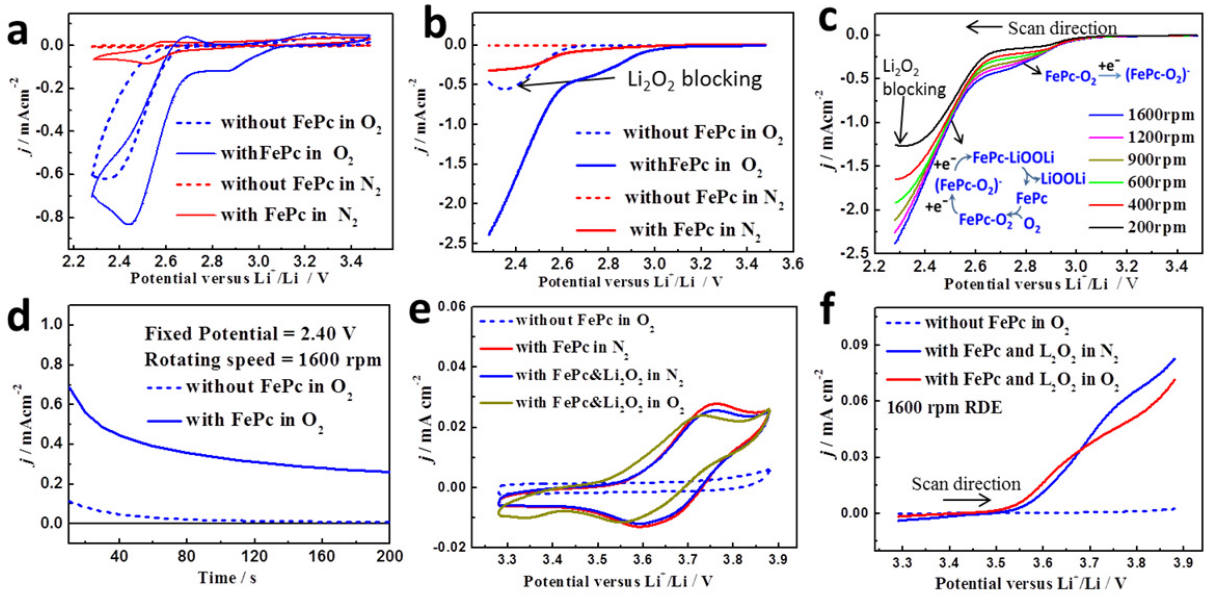

Figure 2. (**a**,**b**) ORR potential range CV(**a**) and fixed speed RDE(**b**) measurement of the DMSO-LiTFSI electrolytes with/without FePc in inert/oxygen atmosphere. (**c**) Changing the speed of the RDE measurement of the DMSO-LiTFSI electrolyte with FePc in oxygen atmosphere. (**d**) Current decrease with different electrolytes in fixed potential RDE measurement. (**e&f**) OER potential range CV(**e**) and RDE(**f**) measurement of the DMSO-LiTFSI electrolytes with/without $FePc/Li_2O_2$ powder. CV potential scan rate=50 mV s^{-1}, RDE potential scan rate=5 mV s^{-1}.

Catalytic activity of FePc in lithium-oxygen batteries

We tested the catalytic activity of FePc dissolved in oxygen-containing TEGDME or DMSO electrolyte with a cathode composed of carbon fibers (CFs). Initially, no solid catalyst existed on the CFs. For comparison, we tested the catalytic activity at a CF cathode with a solid Fe-N/C catalyst but no FePc dissolved in the electrolyte. The solid Fe-N/C is a well-known solid catalyst for the ORR[1,15-17,35]. Finally, we tested a cathode with Fe-N/C attached onto the CFs and FePc in the electrolyte.

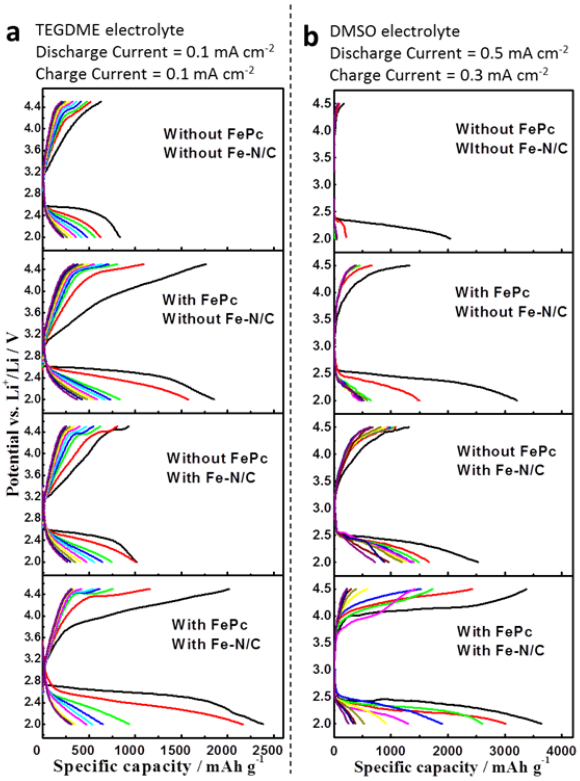

Figure 3. (**a&b**) The effects of different catalysts on the discharge-charge performance with TEGDME (**a**) or DMSO (**b**) based electrolytes.

The CFs were obtained by carbonization of an electrospun mixture of polyacryulonitrile (PAN) and polymethylmethacylate (PMMA) fibers[44]. (Fig. S3) The composition of the CFs can be easily modified by adding precursors into the electrospinning solution, which allows us to fabricate morphologically similar CFs with and without a solid state catalyst. We incorporated the solid Fe-N/C catalyst into the CFs by adding FePc into the polymer solution before electrospinning and carbonization. Energy dispersive X-ray spectroscopy (EDX, Fig. S4) and X-ray photoelectron spectroscopy (XPS, Fig. S5) results indicate the composition of our Fe-N/C CFs composite is comparable to that of Fe-N/C catalyst previously reported for a lithium-air battery[17].

Fig. 3 compares the half-cell discharge/charge voltage profiles for the CFs with different catalysts and different electrolyte solvents. We noticed that dissolved FePc showed obvious catalytic activity toward both ORR and OER processes. Much improved discharge capacity and lower charge potential were obtained in both TEGDME and DMSO electrolytes by adding FePc. Because the viscosity of the DMSO was lower than the TEGDME, the DMSO based batteries were able to tolerate higher discharge and charge current density. Furthermore, the dissolved FePc and solid Fe-N/C catalysts are compatible and work synergistically. The batteries' performance attained to the best when both of the FePc and the Fe-N/C were used.

Interestingly, the FePc changed the morphology of the Li_2O_2 product of the discharge (Fig. 4). Without the FePc, the Li_2O_2 formed during discharge covers the surface of the CFs (Fig. 4b) whereas with the FePc in solution, Li_2O_2 deposited not only on the CF surface, but also on the Li_2O_2 itself until the Li_2O_2 almost fills the space between the CFs (Fig. 4d). This morphology change demonstrates that with FePc in solution, the deposited Li_2O_2 does not block either the catalytically active surface or the catalytic ORR of the dissolved FePc if it is aggregated into particles. Both SEM and XRD result show that the Li_2O_2 was decomposed after charge, which agrees with the capacity increase and reversibility improvement in Fig.3.

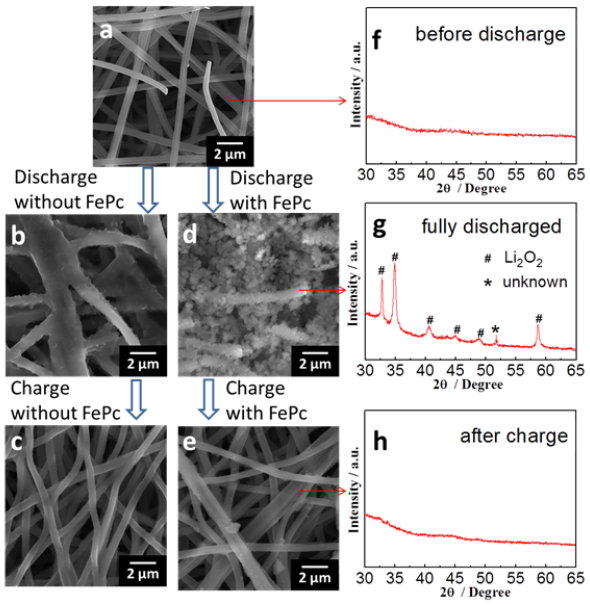

Figure 4. (**a-e**) SEM images of the CF cathodes (with Fe-N/C) before discharge (**a**), after discharge (**b&d**) and after charge (**c&e**) with (**d&e**) and without (**b&c**) FePc catalyst. (**f-h**) XRD pattern of the CF cathode before discharge (**f**), after discharge (**g**) and after charge (**h**) with FePc dissolved in the TEGDME electrolyte.

The replacement of the CFs with a graphene sponge can improve the cathode performance, especially the cyclability, as shown in Fig 5. The graphene sponge is a porous, ultra-light, flexible, conductive material consisting of graphene nanosheets[45] (Fig. 5a). The average space between the graphene nanosheets is about 200 nm, which is much

smaller than the *ca.* 2 μm space between the CFs. The average diffusion distance for the dissolved catalyst is, thereby, shortened considerably.

The cells assembled were tested with a homemade device to suppress the DMSO evaporation (Fig. S6). The discharge and charge capacities were limited to 1000 mAh g^{-1}; the discharge current was 0.5 mA cm^{-2}, the charge current was 0.3 mA cm^{-2}. Without the FePc, the cell failed at the 21st cycle; with the aid of FePc, the discharge curves exhibited a flat plateau at 2.69 V fading only to 2.67 V after 130 cycles. The charge end potential increased steadily over the first 50 cycles and leveled off at about 4.22 V from the 50th to the 130th cycle. The decomposition of electrolyte at high voltage is a major reason of the Li-O_2 battery performance decay. It is very difficult to totally eliminate these side reactions. But since the FePc is effective to lower the charging potential, it should be available to depress the electrolyte decomposition and improve the cyclability.

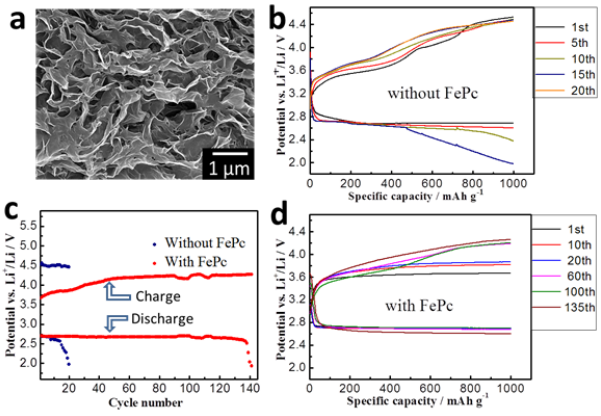

Figure 5. (**a**) SEM image of the graphene sponge. (**b**) Cycle performance of the battery without FePc. (**c**) Cycle performance of the battery with FePc. (**d**) The discharge and charge end potential at different cycles.

Discussion

The catalysis mechanism of the FePc is proposed as follows: As illustrated in Scheme 1a, FePc is a 2D molecule containing low-spin Fe^{II} coordinated by four square-coplanar N atoms; the non-bonding $(3z^2 - r^2)^2$ and $(yz \pm iz)^4$ orbitals are not filled. The non-bonding O-2p orbitals of an O_2 molecule are attracted to the positive core of the exposed Fe^{II} ion. According to Fig. 1, we propose a "(FePc-O_2) → (FePc-O_2)$^-$ →(FePc-LiOOLi)" two-step transformation mechanism. The (FePc-LiOOLi) would diffuse to a nucleated Li_2O_2 site, and then the LiOOLi part would separate from the FePc and incorporate into the crystal lattice of the Li_2O_2. In this process, the FePc-O_2 molecule serves as a shuttle of electrons from the carbon where it forms (FePc-LiOOLi) to a nucleated solid Li_2O_2 site where the Li_2O_2 grows. Such a process is consistent with the RDE data (Fig. 2) and the SEM observation (Fig. 4).

To apply this model to the reverse reaction on charge, we look back Fig. 2e. The reduction potential of oxidized FePc (3.55 V) is higher than the oxidation potential of LiOOLi (3.25 V), indicating that the Fe^{III} of $(FePc)^+$ can oxidize the $(O_2)^{2-}$ molecule of Li_2O_2 to reform (FePc-O_2)$^-$. The (FePc-O_2)$^-$ can diffuse back through the electrolyte to the carbon surface to be further oxidized into FePc and O_2. It is the energy of the Fe^{III}/Fe^{II} couple in the FePc molecule that allows oxidation of the Li_2O_2, and it is the ability of the solution-based FePc$(O_2)^-$ molecule to shuttle from the Li_2O_2 particles to near enough to the carbon surface for electron transfer that makes possible the OER (Scheme 1b).

Scheme 1 The possible catalyzed reaction routes

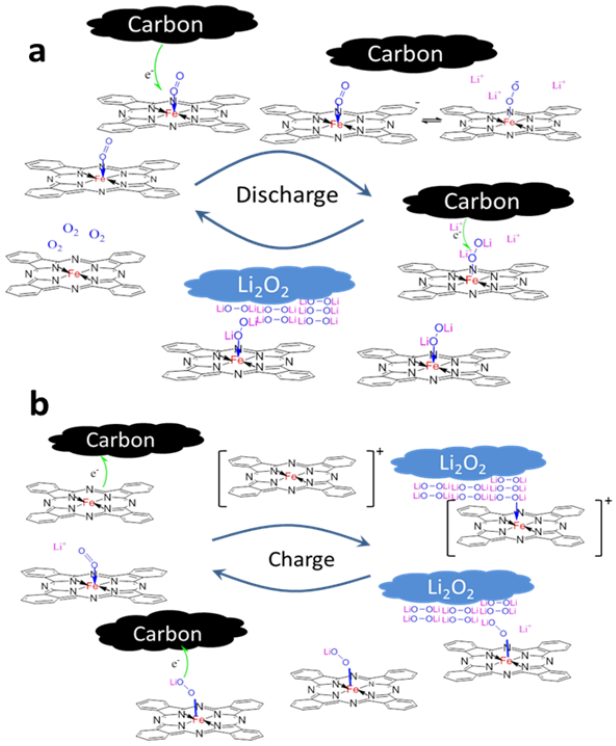

There are many differences between the solution-phase and solid-phase catalysts used in lithium-oxygen batteries, as listed in Table 1. In the ORR, the solution-phase catalyst transports the insulating Li_2O_2 product away from the carbon surface to prevent it from blocking the electron transfer need to reduce the O_2. In the OER, the reactive sites of the solution-phase catalyst can be anywhere at the Li_2O_2 surface because of its diffusion. The contact between the solution-phase catalyst and the solid Li_2O_2 reactant is much better than that between the Li_2O_2 and a solid catalyst. But the electronic conductivity of the solution-phase catalysts is not as good as the solid-phase catalysts. So the solid-phase catalysts still have their own advantages on catalyzing reactions on its surface. Other than direct carbon-catalyst-reactant electron transfer, solution-phase catalysis involves some molecular shuttling through the electrolyte[32,46]. Thus, the diffusion rate and the average diffusion distance of the catalyst-reactant

complexes may influence the total catalysis efficiency. Electrolytes with lower viscosity and cathode materials with smaller pore size are more favorable. It should also be noticed that the FePc is an oxygen carrier and enhanced the solubility of oxygen. This is very good for both solution phase and solid phase catalysis.

Table 1 Comparison of the solution phase catalyst and solid phase catalyst in lithium-air batteries

Catalyst type	Solution phase	Solid phase
Catalyst-reactant contact	Good	Not good
Reactions without carbon contact	Yes	No
Electronic conductivity	Poor	Good
Molecular shuttle effect	Yes	No
Oxygen carrier	Yes	No
Influence to the anode	Yes	No

As the FePc is dissolved in the electrolyte, it is possible to diffuse to the anode and cause some unfavorable side reactions. In organic electrolyte lithium-air batteries, the solid electrolyte interphase (SEI) layer is an effective shield to prevent the oxygen-lithium direct contact[38,47] and slow down the anode direct oxidation rate to a tolerable level. In our case, the molecule size of FePc-oxygen is larger that of free oxygen, so it is more likely to be separated by the SEI. We disassembled two batteries with and without FePc after 10 cycles to see the stability of the lithium anode (Fig. 6). The red circles in the figure indicate the area covered by the air cathode. The whole lithium anode was covered by the electrolyte wetted separator. The area out of the red circles was still shining, showing that the lithium anode is stable when steadily exposed in FePc-containing electrolyte and pure oxygen atmosphere. The area inside the red circles became dark for both FePc-containing and FePc-absent samples, which is because the SEI was damaged in the cycling process and the lithium dendrites might form and be oxidized. Some FePc may react or chemically adsorb on the anode surface. The analysis based on ICP-AES (inductively coupled plasma - atomic emission spectrometer) shows that the amount of Fe element on the anode after 10 cycles was about 1.7×10^{-9} mol, which was 11% of the original FePc total amount in the electrolyte. This effect may cause some FePc concentration decrease in the electrolyte and suppress the catalytic efficiency, but it should not be very serious. The overall life time of FePc-containing batteries were much longer than the FePc-absent batteries. This means that the influence of the FePc to the anode is tolerable[48]. To better solve this anode problem, we will need a more stable SEI layer or a thin oxide/polymer Li^+-electrolyte separator[49] that blocks dendrites from a lithium anode and migration of FePc from the cathode to the anode.

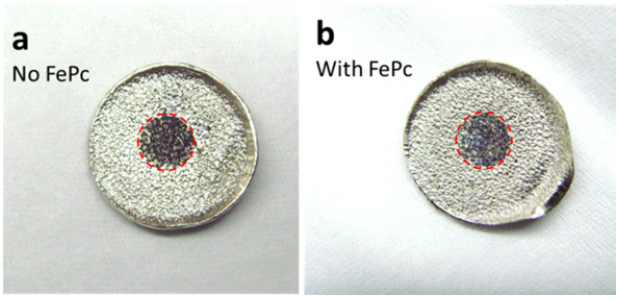

Figure 6. Photo of the lithium anodes taken out of the coin cells after 10 cycles at 1000 mAh g^{-1}.

Conclusion

The FePc-based solution-phase catalyst has been proven to be effective in the discharge/charge process and to enable a rechargeable lithium-oxygen battery of large capacity. The Fe-oxygen coordination and the electron dislocation in the big conjugated structure lowers the energy of the high energy intermediates in the ORR and OER. The dissolved FePc can act as a molecular shuttle of $(O_2)^-$ species and electrons between the surface of electronically conducting carbon and product Li_2O_2 particles. As a consequence, the Li_2O_2 is observed to grow and decompose without direct contact with carbon. We show that the synergy of the solid catalyst and the solution-phase shuttle catalyst is critical for achieving a high-capacity reversible lithium-oxygen battery.

Experimental Section

Preparation of the electrolytes. The solvents, TEGDME and DMSO, were purchased from Sigma Aldrich, both were further dried over freshly activated molecular sieves (type 4 Å) for 24 h. Lithium bis(trifluoromethane sulfonimide) (LiTFSI) was used as the lithium salt and was dried for 24 h in a vacuum chamber (pressure < 10^{-4} Pa) connected to the glove box filled with Ar. The FePc (from Sigma Aldrich) was also vacuum dried. The electrolytes were prepared by mixing the solvent, LiTFSI and FePc in the Ar glove box. The concentration of the LiTFSI and FePc were controlled at 0.1 mol L^{-1} and 0.002 mol L^{-1}, respectively.

Cyclic voltammetry (CV) & rotating disk electrode (RDE) measurement. The CV and RDE tests were performed on an electrochemical workstation (CHI760E, CH Instruments, Shanghai, China) with a rotating disk electrode system (Pine Research Instrumentation, USA). A glassy carbon disk electrode with 5 mm diameter was used as the working electrode. A piece of stainless steel mesh loaded with half charged $LiFePO_4$ was used as the counter electrode. A standard calomel electrode (SCE) with a double bridge was used as the reference electrode. The electrolyte, composed of 0.1 mol l^{-1} LiTFSI and 0.002 mol l^{-1} FePc in DMSO solution, was prepared in the argon-filled glove box. Nitrogen was induced to the electrolyte for 30 min to ensure the data measured in inert atmosphere. Then, pure oxygen was purged into the electrolyte for 10 min to study the ORR. Solid lithium perox-

ide powder was added to the electrolytic cell while stirring before use for the OER study.

Synthesis of the carbon fibers (CFs). 1 g PAN (M_w = 150,000 g mol^{-1}, ALDRICH Co.) and 0.5 g PMMA (M_w = 99,100 g mol^{-1}) were dissolved in 10 ml dimethylformamide (DMF) under magnetic stirring at 60 °C for at least 24 h to obtain a homogenous solution. Then the solution was transferred into a syringe with a 22 blunt needle. Electrospinning was carried out at 15 KV with a pump rate of 5 μl min^{-1}. The as-obtained electrospinning PAN/PMMA nanofibers were stabilized in air for 6 h at 280 °C then carbonized in N_2 at 650 °C for 3 h. After being cooled to room temperature the CFs were obtained. CFs with Fe-N/C were prepared according to the same procedures but with the addition of 0.1 g FePc (M_w = 568.37 g mol^{-1}, ALDRICH Co.) into the polymer solution before electrospinning.

Synthesis of the graphene sponge. Graphite flakes with average size of 500 μm were used to synthesis graphene oxide (GO) according to the previously reported process[50]. A scheme of the fabrication of the sponge with uniform thickness is shown as Fig. S7.

Lithium-oxygen battery assembly. Lithium-oxygen batteries were assembled in an argon-filled glove box with oxygen and water contents less than 1 ppm. The batteries have a coin cell structure, consists of a stainless steel anode shell, a metallic lithium foil anode (0.5 mm thick), a Celgard 3501 separator (from Celgard LLC), as-synthesized carbon cathode (CF or graphene sponge), a nickel foam current collector and a stainless steel cathode shell with holes on it. The lithium foil was treated with 0.1 mol l^{-1} $LiClO_4$-propylene carbonate (PC) solution for at least 3 days before usage to form an SEI layer to protect the anode. A homemade device may be added to depress the DMSO evaporation (Figure S6). The cathode loading density was about 1 mg cm^{-2} for CFs or 0.25 mg cm^{-2} for graphene sponges. The amount of the electrolyte was 8 μL.

Electrochemical performance test. The galvanostatic discharge and charge tests were conducted on a LAND CT2001A battery system.

XRD、SEM、EDX、XPS characterizations. The discharge and charge products were washed with pure DMSO before characterization. The XRD test was conducted with a rotating copper Kα radiation (PANalytical B.V., Holland). EDX and SEM data were obtained with a SIRION200 SEM machine. The XPS experiment was performed on an ESCALAB 250Xi XPS system with a monochromatic Al X-ray source (1486.6 eV).

ICP-AES analysis. The amount of Fe element adsorbed on the Li anode after 10 cycles of discharge/charge at 1000 mAh g^{-1} was measured with ICP-AES (PerkinElmer, Optima4300DV). The whole anode was put into water to make the solution for measurement.

ASSOCIATED CONTENT

Supporting Information. Calculation details, Prove of the Li_2O_2 blocking effect, Characterization of Fe-N/C CFs, Experimental set-ups. This material is available free of charge via the Internet at http://pubs.acs.org.

AUTHOR INFORMATION

Corresponding Author

Dr. Yue Shen: shenyue1213@hust.edu.cn ;
Dr. Yunhui Huang: huangyh@mail.hust.edu.cn

Funding Sources

This work is supported by the Natural Science Foundation of China (51202076, 50825203, 20825520) , China Postdoctoral Science Foundation (2012M510178, 2013T60716), Ministry of Science and Technology of China (2011YQ12003503) and the Robet A. Welch Foundation Grant Number F-1066, Houston, Texas.

Notes

The authors declare no competing financial interests.

ACKNOWLEDGMENT

The authors thank Analytical and Testing Center of HUST for XRD and SEM measurements.

ABBREVIATIONS

FePc, iron phthalocyanine; CF, carbon fiber; TEGDME, tetraethylene glycol dimethyl ether.

REFERENCES

(1)Abraham, K. M.; Jiang, Z. *J. Electrochem. Soc.* **1996**, *143*, 1.
(2)Bruce, P. G.; Freunberger, S. A.; Hardwick, L. J.; Tarascon, J.-M. *Nat. Mater.* **2012**, *11*, 19.
(3)Zhang, T.; Imanishi, N.; Takeda, Y.; Yamamoto, O. *Chem. Lett.* **2011**, *40*, 668.
(4)Lu, Y.-C.; Gallant, B. M.; Kwabi, D. G.; Harding, J. R.; Mitchell, R. R.; Whittingham, M. S.; Shao-Horn, Y. *Energy & Environmental Science* **2013**, *6*, 750.
(5)Cheng, F.; Chen, J. *Chem. Soc. Rev.* **2012**, *41*, 2172.
(6)Shao, Y.; Park, S.; Xiao, J.; Zhang, J.-G.; Wang, Y.; Liu, J. *ACS Catalysis* **2012**, *2*, 844.
(7)Thapa, A. K.; Saimen, K.; Ishihara, T. *Electrochem. Solid-State Lett.* **2010**, *13*, A165.
(8)Lu, Y.-C.; Xu, Z.; Gasteiger, H. A.; Chen, S.; Hamad-Schifferli, K.; Shao-Horn, Y. *J. Am. Chem. Soc.* **2010**, *132*, 12170.
(9)Benbow, E. M.; Kelly, S. P.; Zhao, L.; Reutenauer, J. W.; Suib, S. L. *The Journal of Physical Chemistry C* **2011**, *115*, 22009.
(10)Wang, L.; Zhao, X.; Lu, Y.; Xu, M.; Zhang, D.; Ruoff, R. S.; Stevenson, K. J.; Goodenough, J. B. *J. Electrochem. Soc.* **2011**, *158*, A1379.
(11)Li, J.; Wang, N.; Zhao, Y.; Ding, Y.; Guan, L. *Electrochem. Commun.* **2011**, *13*, 698.
(12)Lim, H.-D.; Gwon, H.; Kim, H.; Kim, S.-W.; Yoon, T.; Choi, J. W.; Oh, S. M.; Kang, K. *Electrochim. Acta* **2013**, *90*, 63.
(13)Yoon, T. H.; Park, Y. J. *Nanoscale Res. Lett.* **2012**, *7*, 28.
(14)Cui, Y.; Wen, Z.; Liu, Y. *Energy & Environmental Science* **2011**, *4*, 4727.
(15)Zhang, S. S.; Ren, X.; Read, J. *Electrochim. Acta* **2011**, *56*, 4544.
(16)Wu, J.; Park, H. W.; Yu, A.; Higgins, D.; Chen, Z. *The Journal of Physical Chemistry C* **2012**, *116*, 9427.
(17)Shui, J.-L.; Karan, N. K.; Balasubramanian, M.; Li, S.-Y.; Liu, D.-J. *J. Am. Chem. Soc.* **2012**, *134*, 16654.
(18)Zhang, T.; Zhou, H. *Angew. Chem. Int. Ed.* **2012**, 51, 11062.
(19)Kitaura, H.; Zhou, H. *Adv. Energy Mater.* **2012**, *2*, 889.
(20)Mitchell, R. R.; Gallant, B. M.; Thompson, C. V.; Shao-Horn, Y. *Energy & Environmental Science* **2011**, *4*, 2952.
(21)Zhang, T.; Zhou, H. *Nat. Commun.* **2013**, *4*, 1817.
(22)Wang, Z.-L.; Xu, D.; Xu, J.-J.; Zhang, L.-L.; Zhang, X.-B. *Adv. Funct. Mater.* **2012**, *22*, 3699.

(23)Sun, B.; Wang, B.; Su, D.; Xiao, L.; Ahn, H.; Wang, G. *Carbon* **2012**, *50*, 727.
(24)Yoo, E.; Nakamura, J.; Zhou, H. *Energy & Environmental Science* **2012**, 5, 6928.
(25)Xiao, J.; Mei, D.; Li, X.; Xu, W.; Wang, D.; Graff, G. L.; Bennett, W. D.; Nie, Z.; Saraf, L. V.; Aksay, I. A.; Liu, J.; Zhang, J.-G. *Nano Lett.* **2011**, *11*, 5071.
(26)Xu, J.-J.; Xu, D.; Wang, Z.-L.; Wang, H.-G.; Zhang, L.-L.; Zhang, X.-B. *Angew. Chem. Int. Ed.* **2013**, 52, 3887.
(27)Zhao, Y.; Xu, L.; Mai, L.; Han, C.; An, Q.; Xu, X.; Liu, X.; Zhang, Q. *Proc. Natl. Acad. Sci.* **2012**, *109*, 19569.
(28)Oh, S. H.; Black, R.; Pomerantseva, E.; Lee, J.-H.; Nazar, L. F. *Nat. Chem.* **2012**, *4*, 1004.
(29)Shao, Y.; Ding, F.; Xiao, J.; Zhang, J.; Xu, W.; Park, S.; Zhang, J.-G.; Wang, Y.; Liu, J. *Adv. Funct. Mater.* **2013**, *23*, 987.
(30)Trahan, M. J.; Mukerjee, S.; Plichta, E. J.; Hendrickson, M. A.; Abraham, K. M. *J. Electrochem. Soc.* **2013**, *160*, A259.
(31)McCloskey, B. D.; Scheffler, R.; Speidel, A.; Bethune, D. S.; Shelby, R. M.; Luntz, A. C. *J. Am. Chem. Soc.* **2011**, *133*, 18038.
(32)Chen, Y.; Freunberger, S. A.; Peng, Z.; Fontaine, O.; Bruce, P. G. *Nat. Chem.* **2013**, 5, 489.
(33)Lim, H.-D.; Song, H.; Kim, J.; Gwon, H.; Bae, Y.; Park, K.-Y.; Hong, J.; Kim, H.; Kim, T.; Kim, Y. H.; Lepró, X.; Ovalle-Robles, R.; Baughman, R. H.; Kang, K. *Angew. Chem. Int. Ed.* **2014**, *53*, 3926.
(34)Jahnke, H.; Schonborn, M.; Zimmermann, G. *Top. Curr. Chem.* **1976**, *61*, 133.
(35)Bezerra, C. W. B.; Zhang, L.; Lee, K.; Liu, H.; Marques, A. L. B.; Marques, E. P.; Wang, H.; Zhang, J. *Electrochim. Acta* **2008**, *53*, 4937.
(36)He, Q.; Mugadza, T.; Kang, X.; Zhu, X.; Chen, S.; Kerr, J.; Nyokong, T. *J. Power Sources* **2012**, *216*, 67.
(37)Cao, R.; Thapa, R.; Kim, H.; Xu, X.; Gyu Kim, M.; Li, Q.; Park, N.; Liu, M.; Cho, J. *Nat. Commun.* **2013**, *4*.
(38)Peng, Z.; Freunberger, S. A.; Chen, Y.; Bruce, P. G. *Science* **2012**, *337*, 563.
(39)Laoire, C.; Mukerjee, S.; Plichta, E. J.; Hendrickson, M. A.; Abraham, K. M. *J. Electrochem. Soc.* **2011**, *158*, A302.
(40)Jung, H.-G.; Hassoun, J.; Park, J.-B.; Sun, Y.-K.; Scrosati, B. *Nat. Chem.* **2012**, *4*, 579.
(41)C.Leznoff, C.; B, L. A. In *Phthalocyanine properties and applications*; VCH Publishers, Inc: New York, 1989, p 397.
(42)Lever, A. B. P.; Wilshire, J. P. *Inorg. Chem.* **1978**, *17*, 1145.
(43)Yin, G. *Coord. Chem. Rev.* **2010**, *254*, 1826.
(44)Zussman, E.; Yarin, A. L.; Bazilevsky, A. V.; Avrahami, R.; Feldman, M. *Adv. Mater.* **2006**, *18*, 348.
(45)Sun, H.; Xu, Z.; Gao, C. *Adv. Mater.* **2013**, *25*, 2554.
(46)Lacey, M. J.; Frith, J. T.; Owen, J. R. *Electrochem. Commun.* **2013**, *26*, 74.
(47)Younesi, R.; Hahlin, M.; Roberts, M.; Edström, K. *J. Power Sources* **2013**, *225*, 40.
(48)Shui, J.-L.; Okasinski, J. S.; Kenesei, P.; Dobbs, H. A.; Zhao, D.; Almer, J. D.; Liu, D.-J. *Nat. Commun.* **2013**, *4*, 2255.
(49)Knauth, P. *Solid State Ionics* **2009**, *180*, 911.
(50)Xu, Z.; Sun, H.; Zhao, X.; Gao, C. *Adv. Mater.* **2013**, *25*, 188.

SYNOPSIS TOC

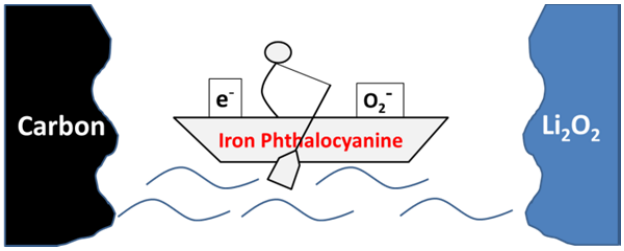

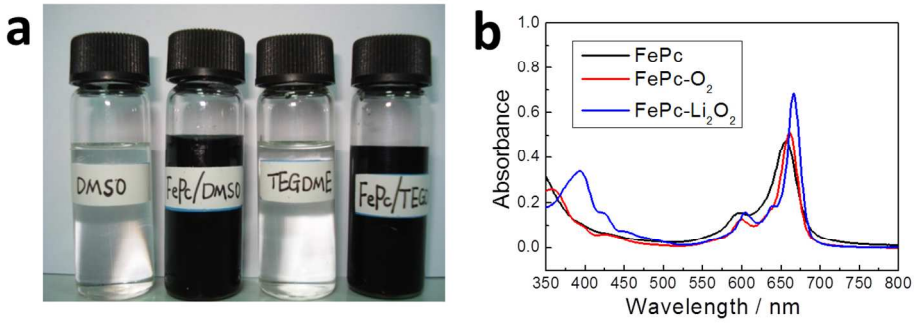

Figure 1. The electrochemical properties of FePc. (a) Photo of the DMSO and TEGDME electrolytes with or without 0.002 mol L-1 FePc. (b) UV-Vis absorption spectra of the FePc, FePc-O2 and FePc-LiOOLi (1.5 x 10-5 mol L-1).
124x44mm (300 x 300 DPI)

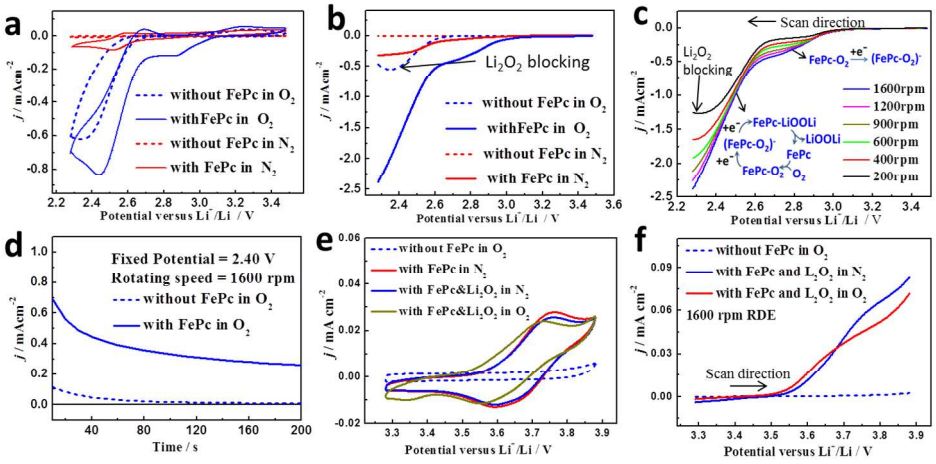

Figure 2. (a,b) ORR potential range CV(a) and fixed speed RDE(b) measurement of the DMSO-LiTFSI electrolytes with/without FePc in inert/oxygen atmosphere. (c) Changing the speed of the RDE measurement of the DMSO-LiTFSI electrolyte with FePc in oxygen atmosphere. (d) Current decrease with different electrolytes in fixed potential RDE measurement. (e&f) OER potential range CV(e) and RDE(f) measurement of the DMSO-LiTFSI electrolytes with/without FePc/Li2O2 powder. CV potential scan rate=50 mV s-1, RDE potential scan rate=5 mV s-1.
131x64mm (300 x 300 DPI)

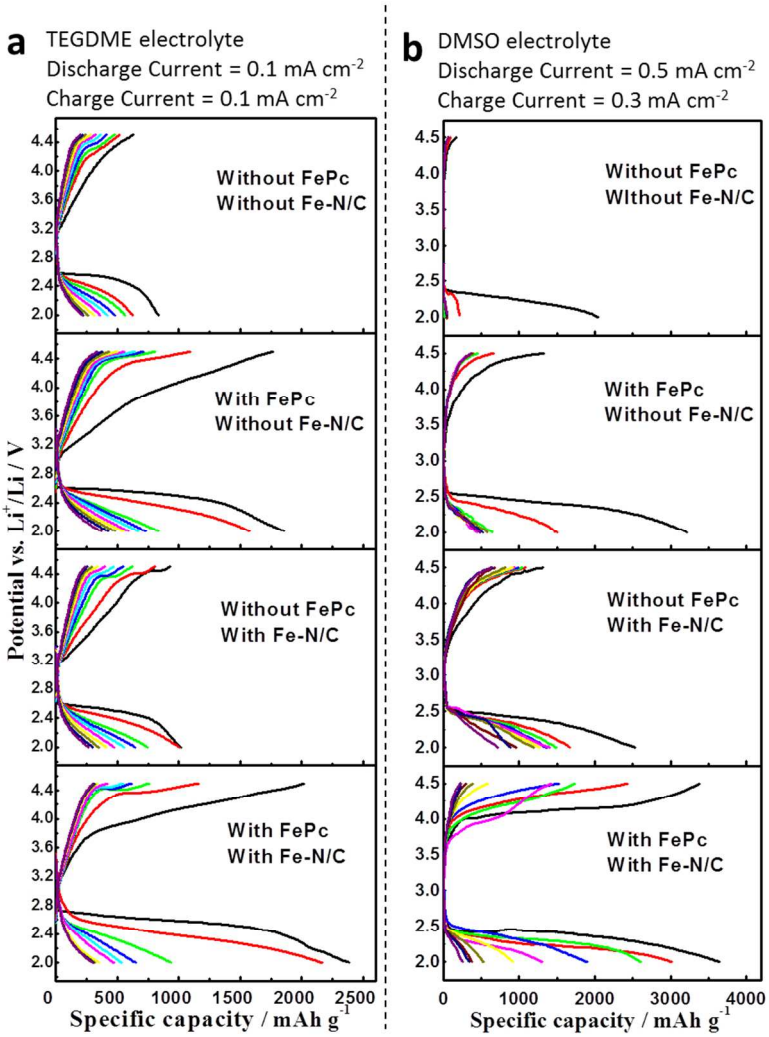

Figure 3. (a&b) The effects of different catalysts on the discharge-charge performance with TEGDME (a) or DMSO (b) based electrolytes.
80x121mm (300 x 300 DPI)

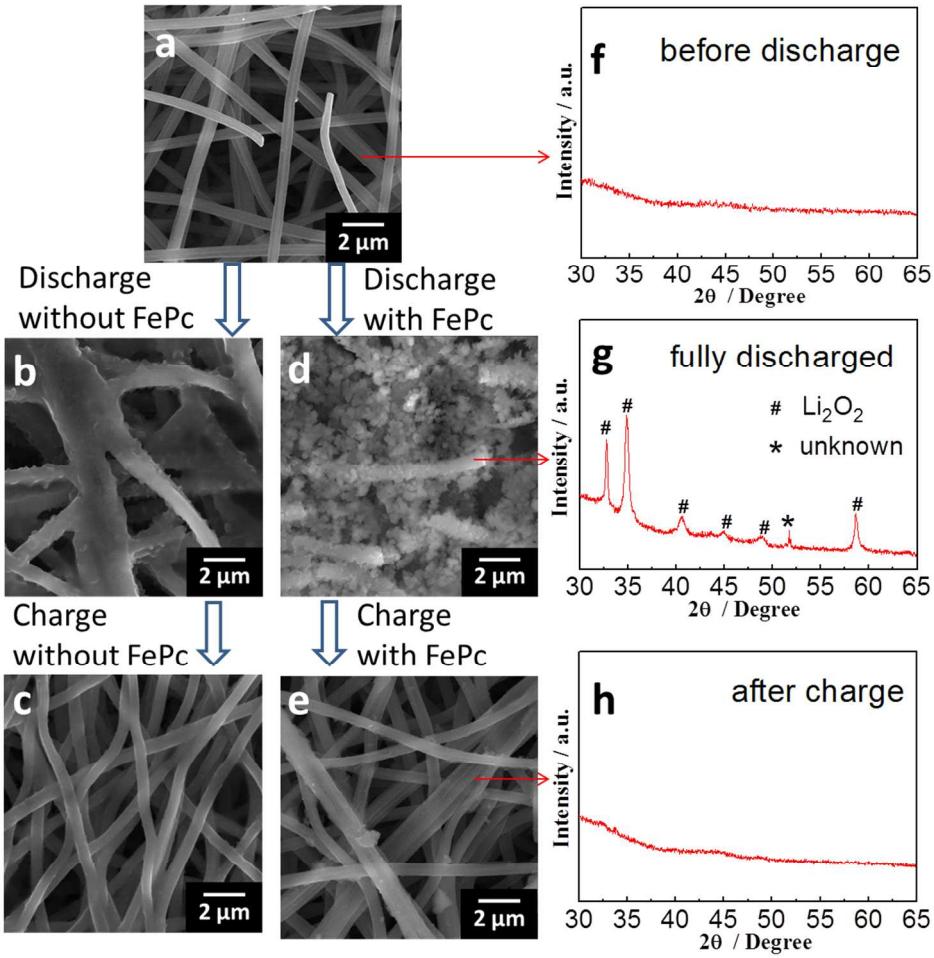

Figure 4. (a-e) SEM images of the CF cathodes (with Fe-N/C) before discharge (a), after discharge (b&d) and after charge (c&e) with (d&e) and without (b&c) FePc catalyst. (f-h) XRD pattern of the CF cathode before discharge (f), after discharge (g) and after charge (h) with FePc dissolved in the TEGDME electrolyte.
105x104mm (300 x 300 DPI)

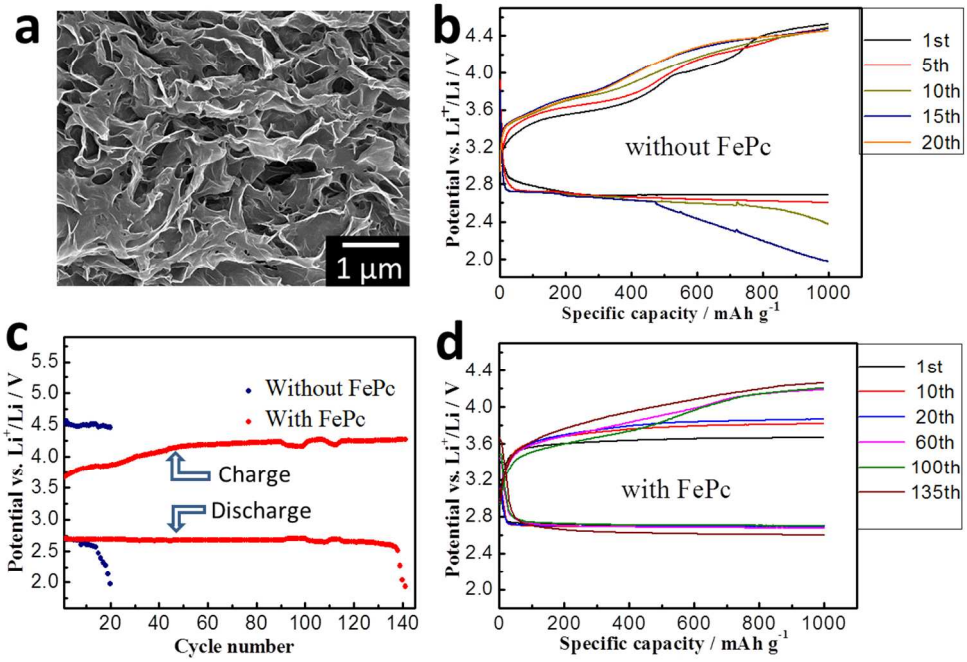

Figure 5. (a) SEM image of the graphene sponge. (b) Cycle performance of the battery without FePc. (c) Cycle performance of the battery with FePc. (d) The discharge and charge end potential at different cycles.
110x78mm (300 x 300 DPI)

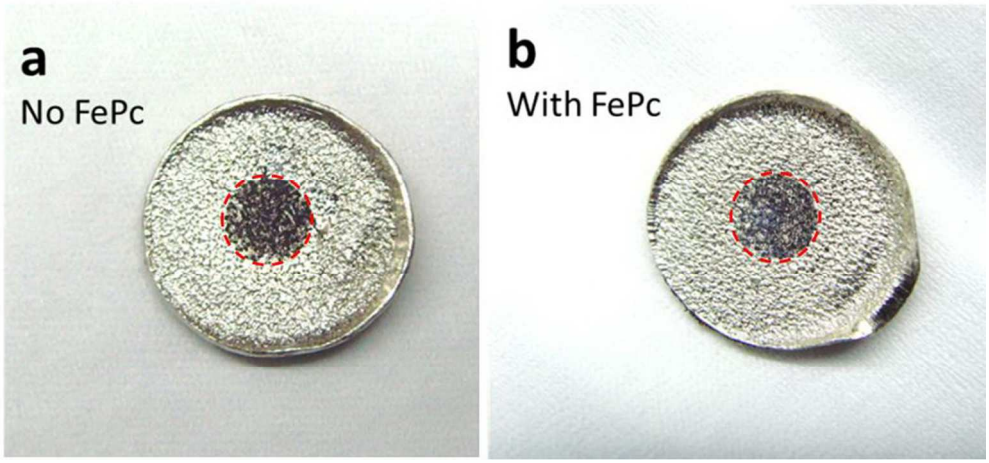

Figure 6. Photo of the lithium anodes taken out of the coin cells after 10 cycles at 1000 mAh g-1.
89x41mm (300 x 300 DPI)

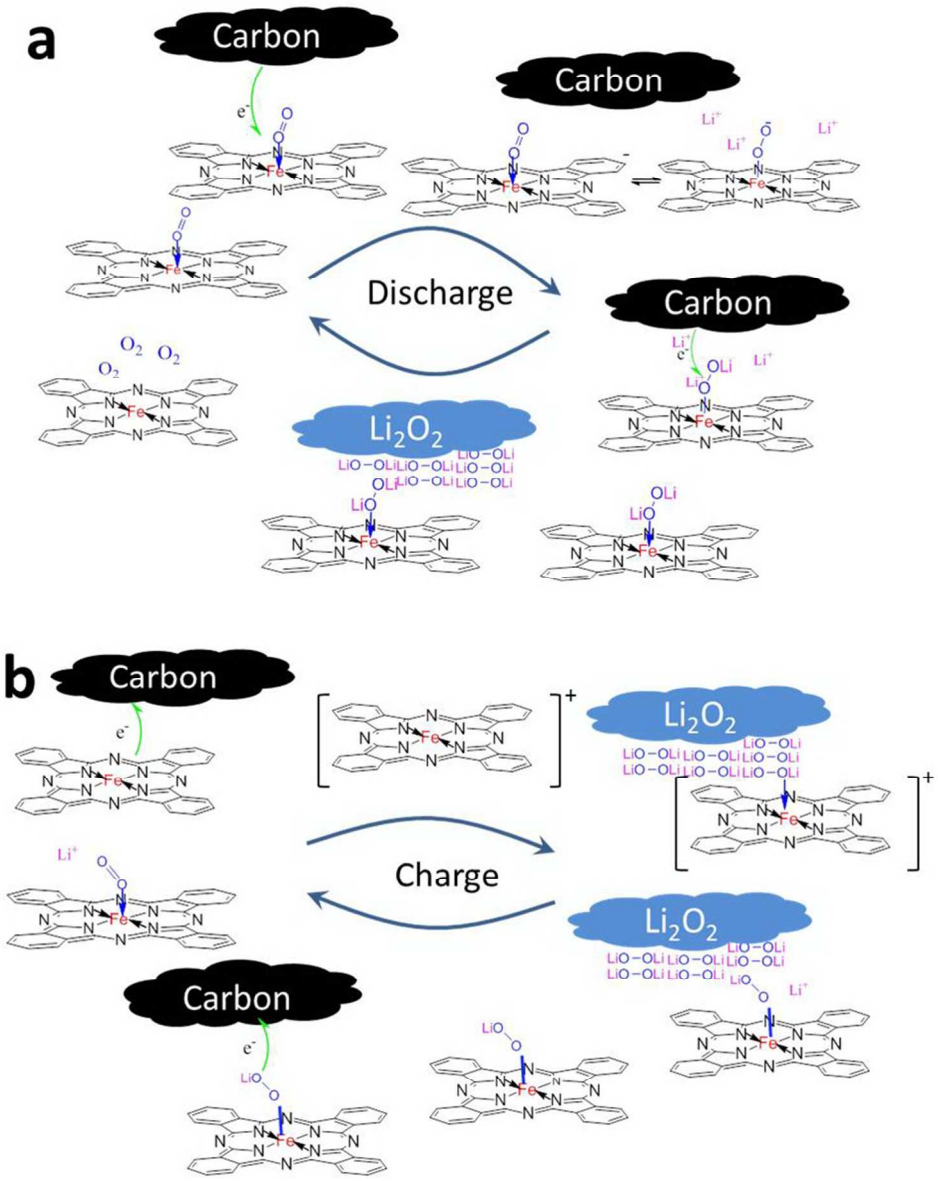

Scheme 1 The possible catalyzed reaction routes
84x103mm (300 x 300 DPI)